Journal of the American Chemical Society

Supporting Information

Experimental and Computational Study of BODIPY Dye-Labeled Cavitand Dynamics

Igor Pochorovski, Tim Knehans, Daniel Nettels, Astrid M. Müller, W. Bernd Schweizer, Amedeo Caflisch, Benjamin Schuler, François Diederich

Table of Contents

1 Synthesis Section

1.1 Synthetic Schemes

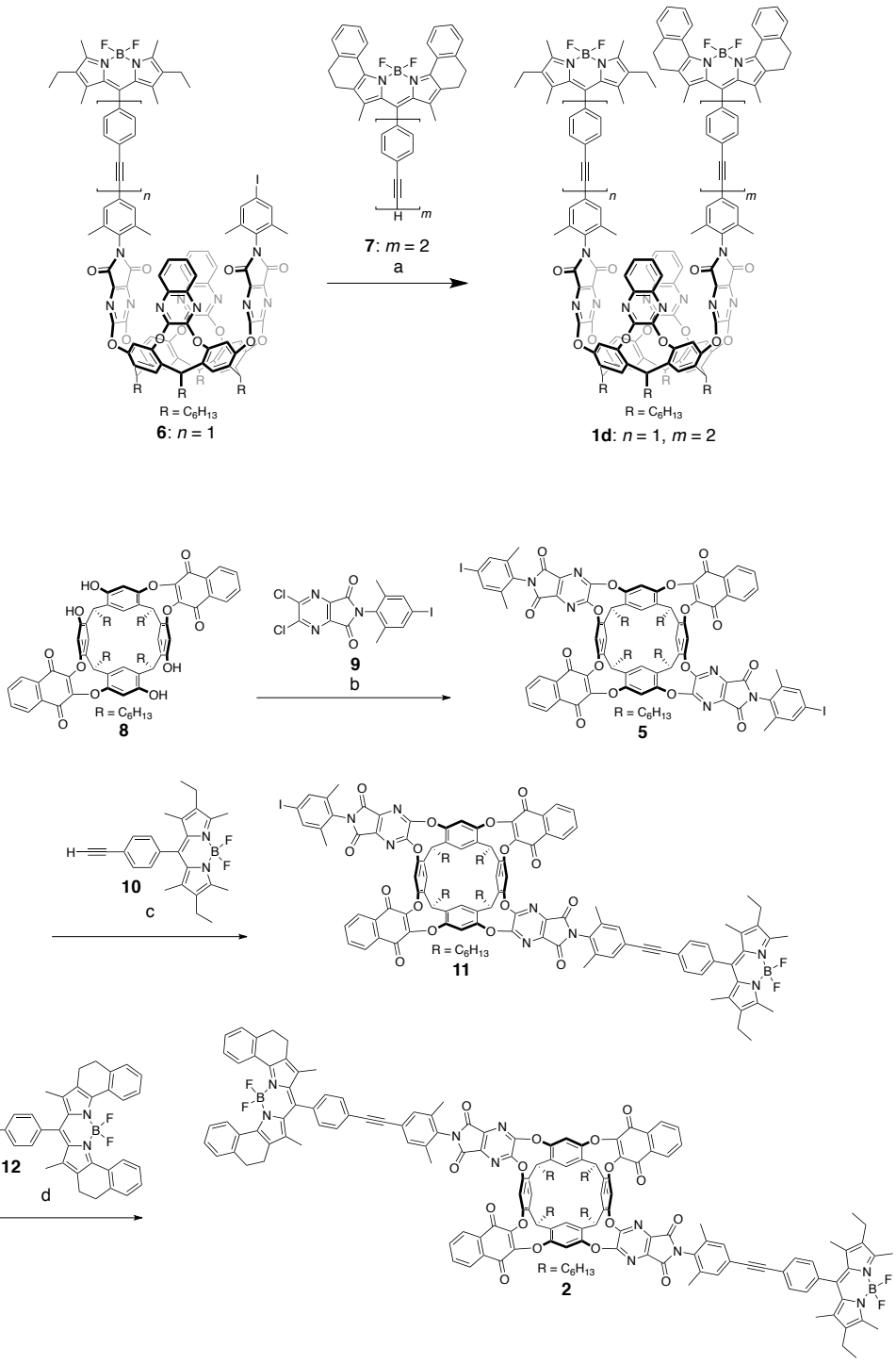

Figure S1. Synthesis of BODIPY dye-substituted cavitands **1d** and **2**. a) [Pd(PPh$_3$)$_4$}], CuI, *i*-Pr$_2$NEt, THF, 35 °C, 2 d; 37%. b) Cs_2CO_3, THF, 70 °C, 24 h; 77%. c) [Pd(PPh$_3$)$_4$}], CuI, *i*-Pr$_2$NEt, THF, 25 °C, 3 d; 17%. d) [Pd(PPh$_3$)$_4$}], CuI, *i*-Pr$_2$NEt, THF, 35 °C, 3 d; 11%.

1.2 Materials and General Methods

All chemicals were purchased as reagent grade and used without further purification. When stated, solvents were degassed by bubbling Ar through the solution for 30 min. Flash chromatography (FC) was performed using SiO_2-60 (230–400 mesh ASTM, 0.040–0.063 mm; Fluka) or SiO_2-F60 (0.040–0.063 mm, 60 Å, Silicycle). Preparative recycling gel permeation chromatography (GPC) was run on a Japan Analytical Industries LC-9101 preparative recycling HPLC apparatus using HPLC-grade $CHCl_3$ as the mobile phase. Melting points were measured on a Büchi B-540 melting-point apparatus in open capillaries. ^{1}H NMR, ^{13}C NMR, and ^{19}F NMR spectra were recorded on a Bruker DRX 400 or Bruker AV 400 spectrometer at 298 K. Residual solvent peaks were used as internal references. ATR Infrared spectra (IR) were recorded on a Varian 800 FT-IR spectrometer. Selected absorption bands are reported in wavenumbers (cm^{-1}). Mass spectrometry was performed by the MS-service at ETH Zürich. High-resolution electron impact mass spectra were measured on a Waters Micromass AutoSpec Ultima spectrometer. High-resolution matrix-assisted laser-desorption-ionization mass spectra were measured on a Varion Ionspec Ultima MALDI-FTICR mass spectrometer using 3-hydroxypyridine-2-carboxylic acid (3-HPA) as matrix or on Bruker Daltonics Ultraflex II MALDI-TOF mass spectrometer using (2-[(2E)-3-(4-t-butylphenyl)-2-methylprop-2-enylidene]malononitril) (DCTB) as matrix. High-resolution electro-spray-ionisation mass spectra were measured on a Bruker Daltonics maXis spectrometer. UV/Vis spectroscopy was carried out with a Varian Cary 500 Scan spectrophotometer. Steady state fluorescence spectroscopy was carried out with an Instruments S. A. Fluorolog-3 spectrofluorimeter. Both UV/Vis and fluorescence experiments were carried out in standard 3.5 mL quartz cells (4 optical windows for UV/Vis, 2 optical windows for fluorescence) with 10 mm path length.

1.3 Synthetic Procedures

Compounds **6**[1], **7**[1-2], **8**[3], **9**[1-2], **10**[1-2], and **12**[1-2] were prepared according to literature procedures.

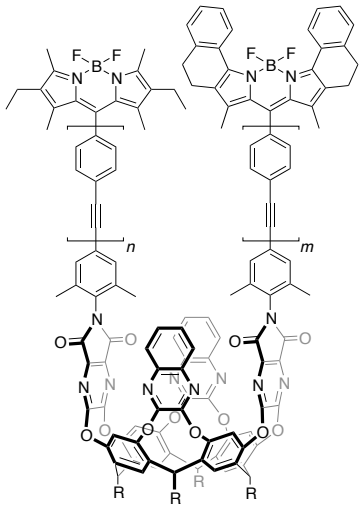

Cavitand 1d

[$Pd(PPh_3)_4$] (19 mg, 0.016 mmol) and CuI (3 mg, 0.016 mmol) were added to a degassed solution of **6** (76 mg, 0.121 mmol), **7** (0.17 g, 0.081 mmol), and DIPEA (0.28 mL, 1.6 mmol) in THF (5 mL) and $CHCl_3$ (5 mL). The mixture was stirred for 2 d at 35 °C, after which the solvent was evaporated. FC (SiO_2; CH_2Cl_2 → CH_2Cl_2/EtOAc 98:2) and recycling GPC (Jaigel-2H; $CHCl_3$) afforded **1d** (78 mg, 37 %) as a blue solid. ^{1}H NMR (400 MHz, $CDCl_3$): δ = 0.90 – 1.05 (m, 18H), 1.27 – 1.64 (m, 50H), 2.16 – 2.41 (m, 19H), 2.51 – 2.63 (m, 10H), 2.83 – 2.99 (m, 4H), 5.63 (t, J = 8.1, 2H), 5.71 (t, J = 8.1, 2H), 7.26 – 7.64 (m, 26H), 7.70 (d, J = 8.1, 1H), 7.75 (d, J = 8.1, 2H), 7.85 – 7.95 (m, 4H), 8.26 (s, 2H), 8.26 (s, 2H), 8.82 ppm (d, J= 8.0, 2H); ^{13}C NMR (101 MHz, $CDCl_3$): δ = 11.96, 12.33, 12.56, 14.04, 14.60, 17.11, 18.05, 18.06, 18.08, 18.10, 20.49, 22.65, 27.93, 27.96, 29.33, 29.35, 30.53, 31.85, 31.86, 32.16, 32.70, 34.20, 34.30, 89.55, 90.20, 90.25, 90.37, 90.43, 90.97, 118.79, 122.99, 123.24, 123.51, 123.77, 125.02, 125.11, 127.32, 128.05, 128.39, 128.73, 129.02, 129.09, 129.14, 129.36, 129.44, 130.57, 131.21, 131.34, 131.66, 131.72, 131.81, 132.17, 132.29, 132.34, 132.36, 132.43, 133.03, 133.75, 135.70, 135.84, 136.12, 136.13, 136.34, 136.54, 136.86, 137.40, 137.51, 138.14, 138.76, 139.12, 139.82, 140.69, 141.48, 150.95, 152.04, 152.25, 153.09, 154.16, 158.85, 158.87, 161.43 ppm; ^{19}F NMR

(376 MHz, $CDCl_3$): δ = −145.63 (q, J = 31.7, 2F), −134.96 (q, J = 33.2, 2F); IR (ATR): $\tilde{\nu}$ = 2926 (w), 2857 (w), 1741 (m), 1525 (m), 1480 (m), 1442 (w), 1411 (m), 1362 (m), 1326 (s), 1275 (m), 1231 (m), 1191 (s), 1157 (s), 1114 (m), 1082 (s), 978 (m), 898 (m), 837 (m), 792 (w), 761 (s), 709 (m), 688 (m), 626 (w); UV/Vis ($CHCl_3$): λ_{max} (ε) = 530 (69000), 620 nm (110000); HR-MALDI-MS (3-HPA): m/z (%): 2581.1280 (100, $[M-F]^+$, calcd for $C_{164}H_{144}B_2F_3N_{14}O_{12}^+$: 2581.1260).

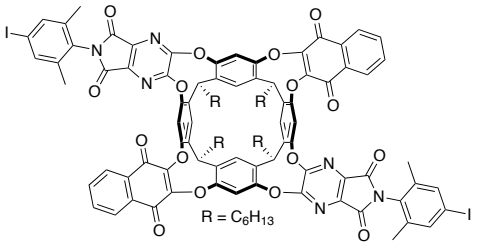

Cavitand 5

Cs_2CO_3 (2.17 g, 6.67 mmol) was added to a solution of tetrol **8** (1.8 g, 1.6 mmol) and iodoimide **9** (1.49 g, 3.34 mmol) in THF (100 mL). The mixture was stirred for 24 h at 70 °C, filtered over silica, and the solvent was evaporated. FC (SiO_2; CH_2Cl_2 → CH_2Cl_2/EtOAc 95:5) afforded **5** (2.3 g, 77 %) as a yellow solid. R_f = 0.48 (SiO_2; CH_2Cl_2/EtOAc 98:2); m.p. > 320 °C (decomp); ^{1}H NMR (400 MHz, $CDCl_3$): δ = 0.79 – 0.96 (m, 12H), 1.21 – 1.41 (m, 32H), 2.01 – 2.15 (m, 14H), 2.17 (s, 6H), 3.68 (t, J = 7.5, 2H), 4.37 (t, J = 7.5, 2H), 6.15 – 7.23 (m, 4H), 7.42 (br s, 4H), 7.57 (s, 2H), 7.60 (s, 2H), 7.65 – 7.80 (m, 4H), 8.02 – 8.26 ppm (m, 4H); ^{13}C NMR (101 MHz, $CDCl_3$): δ = 13.97, 13.99, 17.74, 17.80, 22.52, 22.58, 26.96, 27.05, 29.04, 29.12, 31.49, 31.60, 31.66, 35.55, 37.70, 96.21, 126.76, 128.88, 130.30, 134.35, 137.60, 137.69, 138.84, 139.05, 151.77, 161.78 ppm; IR (ATR): $\tilde{\nu}$ = 2926 (w), 2856 (w), 1795 (w), 1741 (m), 1682 (w), 1605 (w), 1578 (w), 1481 (w), 1351 (s), 1319 (m), 1248 (s), 1197 (s), 1157 (m), 1103 (m), 958 (m), 897 (w), 825 (w), 794 (w), 749 (w), 717 (m), 683 cm^{-1} (w); HR-MALDI-MS (3-HPA): m/z (%): 1884.4403 (100, $[M+H]^+$, calcd for $C_{100}H_{89}I_2O_{16}N_6^+$: 1884.4458).

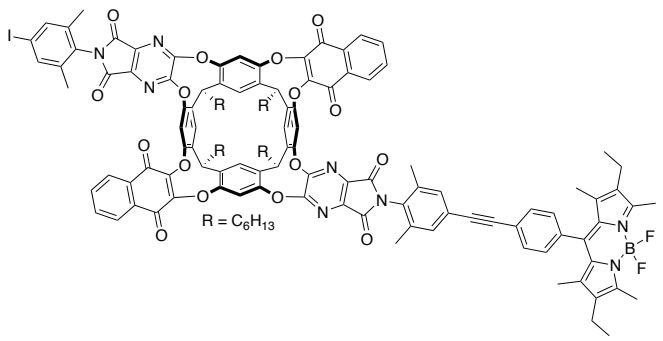

Cavitand 11

$[Pd(PPh_3)_4]$ (46 mg, 0.040 mmol) and CuI (8 mg, 0.04 mmol) were added to a degassed solution of **9** (161 mg, 0.398 mmol), **5** (0.75 g, 0.40 mmol), and DIPEA (1.4 mL, 8.2 mmol) in THF (30 mL). The mixture was stirred for 3 d at 25 °C, after which the solvent was evaporated. FC (SiO_2; CH_2Cl_2 → CH_2Cl_2/EtOAc 97:3) and recycling GPC (Novogrom 100; CH_2Cl_2) afforded **11** (148 mg, 17 %) as a red solid. R_f = 0.57 (SiO_2; CH_2Cl_2/EtOAc 97:3); m.p. > 320 °C (decomp); ^{1}H NMR (400 MHz, $CDCl_3$): δ = 0.84 – 0.93 (m, 12H), 1.02 (t, J = 7.5, 6H), 1.19 – 1.47 (m, 38H), 2.02 – 2.15 (m, 11H), 6.12 – 7.13 (m, 4H), 2.18 (s, 6H), 2.24 (s, 3H), 2.34 (q, J = 7.5, 4H), 2.57 (s, 6H), 3.61 – 3.78 (m, 2H), 4.37 (t, J = 7.4, 2H), 7.32 – 7.36 (m, 2H), 7.37 – 7.54 (m, 6H), 7.57 (s, 1H), 7.60 (s, 1H), 7.66 – 7.71 (m, 2H), 7.71 – 7.77 (m, 4H), 8.07 – 8.22 ppm (m, 4H); ^{13}C NMR (101 MHz, $CDCl_3$): δ = 11.96, 12.56, 13.97, 13.99, 14.63, 17.10, 17.74, 17.80, 18.08, 18.14, 22.52, 22.59, 26.96, 27.05, 29.05, 29.13, 31.50, 31.60, 31.67, 35.55, 37.70, 53.44, 89.67, 89.74, 96.21, 123.60, 124.65, 126.76, 128.57, 128.87, 129.20, 130.30, 130.56, 131.66, 131.78, 132.34, 132.96, 134.31, 136.07, 137.11, 137.31, 137.59, 137.67, 138.25, 138.83, 139.03, 139.21, 151.74, 154.05, 161.76, 161.92 ppm; ^{19}F NMR (377 MHz, $CDCl_3$): δ = −145.77 ppm (q, J = 33.0, 2F); UV/Vis ($CHCl_3$): λ_{max} (ε) = 530 (59000); HR-MALDI-MS (3-HPA): m/z (%): 2139.7494 (100, $[M-F]^+$, calcd for $C_{125}H_{114}BFIN_8O_{16}^+$: 2139.7475).

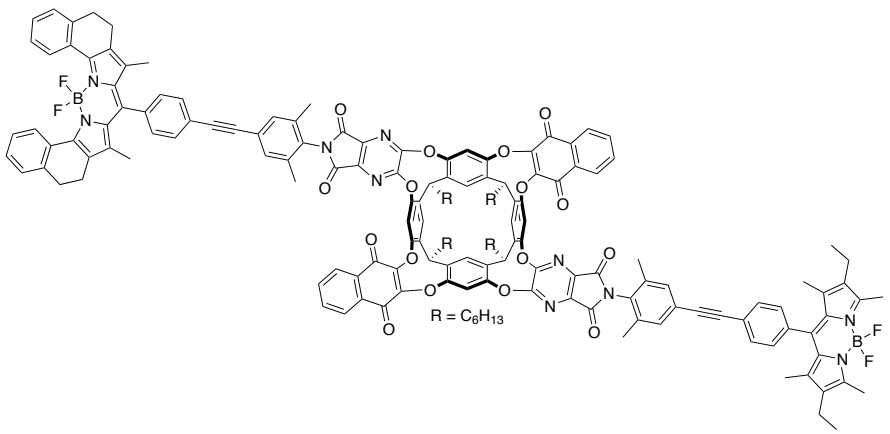

Cavitand 2

$[Pd(PPh_3)_4]$ (11 mg, 0.093 mmol) and CuI (1.7 mg, 0.0093 mmol) were added to a degassed solution of **12** (36 mg, 0.069 mmol), **11** (0.10 g, 0.046 mmol), and DIPEA (0.16 mL, 0.93 mmol) in THF (10 mL). The mixture was stirred for 3 d at 35 °C, after which the solvent was evaporated. FC (SiO_2; CH_2Cl_2 → CH_2Cl_2/EtOAc 97:3) and recycling GPC (Novogrom 100; CH_2Cl_2) afforded **2** (13 mg, 11 %) as a red solid. R_f = 0.57 (SiO_2; CH_2Cl_2/EtOAc 97:3); ^{1}H NMR (400 MHz, $CDCl_3$): δ = 0.89 (q, J = 6.7, 12H), 1.02 (t, J = 7.5, 6H), 1.19 – 1.43 (m, 38H), 1.45 (s, 6H), 2.11 (s, 8H), 2.18 (d, J = 3.4, 6H), 2.25 (d, J = 3.4, 6H), 2.35 (q, J = 7.6, 4H), 2.55 – 2.63 (m, 10H), 2.88 – 2.96 (m, 4H), 3.71 (t, J = 7.2, 2H), 4.38 (t, J = 7.6, 2H), 6.07 – 7.11 (m, 4H), 7.26 – 7.38 (m, 8H), 7.38 – 7.53 (m, 10H), 7.65 – 7.80 (m, 8H), 8.02 – 8.28 (m, 4H), 8.78 – 8.91 ppm (m, 2H); ^{13}C NMR (101 MHz, $CDCl_3$): δ = 11.96, 12.41, 12.56, 13.98, 14.00, 14.63, 17.10, 18.09, 18.15, 20.49, 22.53, 22.59, 26.97, 27.06, 29.05, 29.14, 30.54, 31.51, 31.61, 35.57, 37.72, 53.44, 89.67, 89.74, 89.94, 123.60, 123.86, 124.63, 124.65, 126.77, 127.35, 128.08, 128.38, 128.58, 128.66, 129.04, 129.20, 129.25, 129.46, 130.31, 130.56, 131.68, 131.79, 132.17, 132.34, 132.43, 132.96, 133.75, 135.93, 136.08, 136.41, 137.11, 137.13, 137.33, 137.34, 138.25, 138.82, 140.70, 150.92, 151.75, 154.06, 161.93 ppm; ^{19}F NMR (377 MHz, $CDCl_3$): δ = −145.77 (q, J = 31.8, 2F), −134.97 ppm (q, J = 33.1, 2F); IR (ATR): $\tilde{\nu}$ = 2927 (w), 2857 (w), 1741 (m), 1680 (w), 1607 (w), 1579 (w), 1543 (w), 1480 (m), 1406 (m), 1336 (m), 1263 (m), 1188 (s), 1159 (m), 1084 (m), 959 (m), 897 (w), 796 (w), 774 (w), 715 (m), 648 cm^{-1} (w); UV/Vis ($CHCl_3$): λ_{max} (ε) = 530 (70000), 620 nm (114000); HR-MALDI-MS (3-HPA): m/z (%): 2537.0707 (100, $[M-F]^+$, calcd for $C_{160}H_{140}B_2F_3N_{10}O_{16}^+$: 2537.0621).

1.4 Quantification of Donor-Only Fractions in The Cavitand Samples

Cavitand **1a** had been initially published in 2005, and an unexpectedly high donor fluorescence intensity had been observed in its steady-state fluorescence spectrum.[4] The compound was resynthesized in 2010, together with compound **1b** and **1c**.[1] While the newly synthesized **1a** sample exhibited lower donor fluorescence intensity than the originally published one, it was still too high for assuming a close dye-dye distance.

However, the time-resolved fluorescence spectroscopy results of the current work supported the hypothesis of close dye-dye distances in all cavitands **1a**–**d**. Therefore, we suspicioned that donor-only fractions in the cavitand samples could explain the high donor fluorescence intensities in the steady state fluorescence spectra.

We assumed that the reason for the presence of donor-only fractions is the loss of the BF_2 unit of the acceptor dye during the course of cavitand synthesis, presumably during a TMS-promoted deprotection step of a cavitand dye arm precursor. The larger instability of the acceptor dye compared to the donor dye had been noticed in the SI of reference [2].[1] Loss of the BF_2 unit in BODIPY dyes has precedence and was observed in high acidity media,[5] or under strongly basic conditions.[6] Hints for the partial lack of the BF_2 unit were found in MALDI-MS spectra in the form of $[M–BF_2]^+$ signals (which, however, might also form during the ionization in the mass spectrometer), while no evidence could be drawn from ^1H, ^{13}C, and ^{19}F NMR spectra published in reference [2] for cavitands **1a**–**c**.[1]

Therefore, we obtained new ^{19}F NMR spectra using special conditions (pulse sequence with a 30° flip angle) that allowed quantitative integration of the BF_2 signals, corresponding to the donor and acceptor moieties (see Figure S2). These spectra revealed that cavitands **1a** and **1b** indeed posses significant donor-only portions (18% and 11%, respectively), while cavitands **1c**, **1d**, and **2** show very small donor-only portions that are smaller than the NMR integration error of up to 2%. Due to the small molecular mass difference between the fractions equipped with and lacking the BF_2 unit, separation with gel permeation chromatography (GPC) was not possible. Neither was silica gel chromatography possible due to negligible polarity differences.

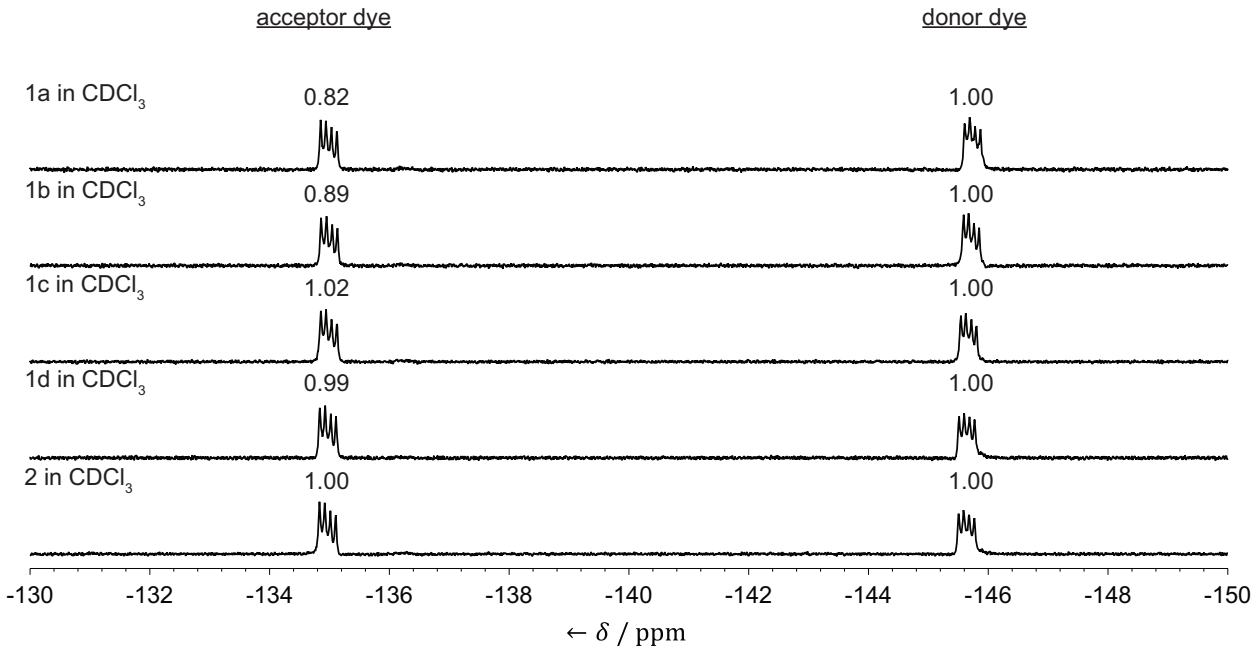

Figure S2. ^{19}F NMR spectra (298 K, 376 MHz) of cavitands **1a**–**d** and **2** in $CDCl_3$ employing a 30° flip angle.

2 X-Ray Data of Cavitand 5

Crystal data for cavitand **5** were deposited with the Cambridge Crystallographic Data Base with CCDC number 953763 ($CDCl_3$, kite), and can be obtained free of charge from The Cambridge Crystallographic Data Centre via www.ccdc.cam.ac.uk/data_request/cif.

A clear yellow prism-like specimen of $C_{115}H_{103}Cl_{45}I_2N_6O_{16}$ (formula weight: 3674.08), approximate dimensions 0.140 mm × 0.240 mm × 0.300 mm, was used for the X-ray crystallographic analysis at 100(2) K. The X-ray intensity data were measured on a Bruker Kappa Apex-II Duo system equipped with a graphite monochromator (λ = 0.71073 Å).

The integration of the data using a monoclinic unit cell yielded a total of 239167 reflections to a maximum θ angle of 27.55° (0.77 Å resolution), of which 67783 were independent (average redundancy 3.528, completeness = 98.9%, R_{int} = 7.89%, R_{sig} = 11.35%) and 33738 (49.77%) were greater than $2\sigma(F^2)$. The index range was: $-35 \le h \le 36$, $-37 \le k \le 27$, $-49 \le l \le 49$. The final cell constants of a = 27.741(2) Å, b = 29.059(3) Å, c = 38.382(3) Å, β = 106.309(4)°, V = 29696.(4) $Å^3$, are based upon the refinement of the XYZ-centroids of 9104 reflections above 20 $\sigma(I^2)$ with 4.422° < 2θ < 53.93°. Data were corrected for absorption effects using the multi-scan method (SADABS). The ratio of minimum to maximum apparent transmission was 0.796. The absorption coefficient is 1.293 mm^{-1}.

The structure was solved by direct methods and refined using the OLEX2 and Bruker SHELXTL Software Package, using the space group P 1 21/n 1, with Z = 8 for the formula unit $C_{115}H_{103}Cl_{45}I_2N_6O_{16}$. The final anisotropic full-matrix least-squares refinement on F^2 with 2049 variables converged at $R1$ = 22.48% ($wR2$ = 54.52%), for the observed data and $R1$ = 32.80% ($wR2$ = 58.43%) for all data. The goodness-of-fit was 3.173. The largest peak in the final difference electron density synthesis was 8.089 e $Å^{-3}$ and the largest hole was −5.517 e $Å^{-3}$ with an RMS deviation of 0.419 e $Å^{-3}$. On the basis of the final model, the calculated density was 1.644 g cm^{-3} and F(000), 14672 e.

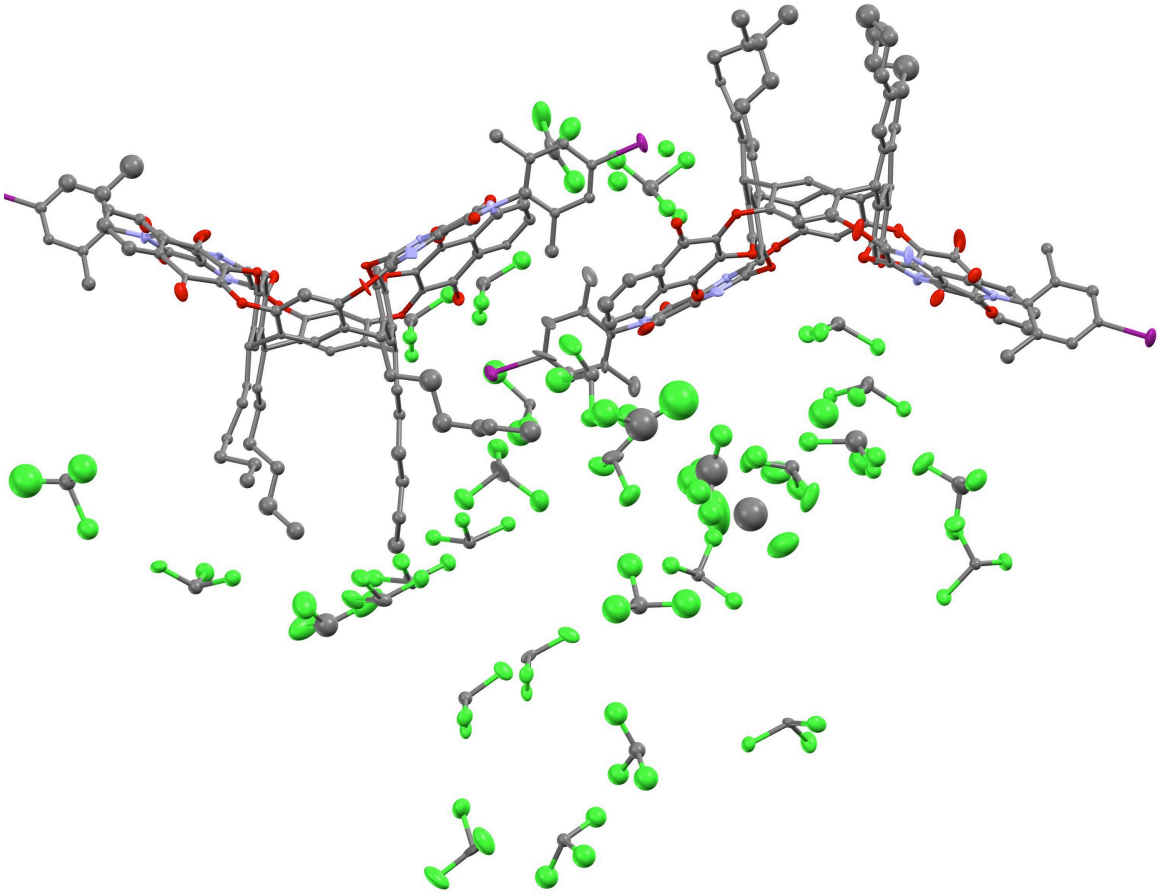

Figure S3. Asymmetric unit of the crystal structure of cavitand **5** (kite, from $CDCl_3$) measured at 100 K. Thermal ellipsoids are shown at the 50% probability level.

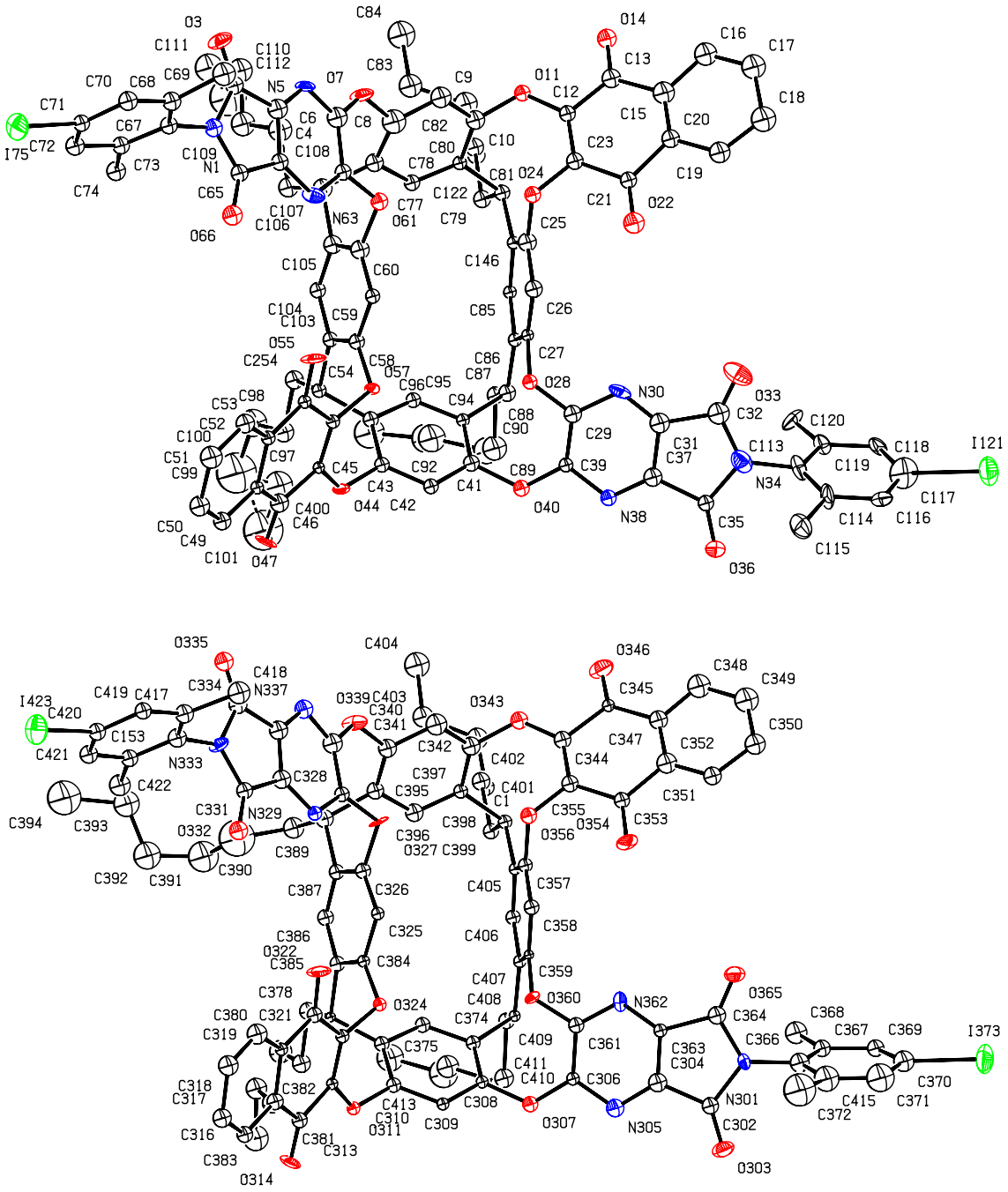

Figure S4. Molecular structures of **5** in the crystal including atom numbers (kite, from $CDCl_3$) measured at 100 K. Thermal ellipsoids are shown at the 50% probability level.

3 Fluorescence Section

3.1 Reference Donor and Acceptor BODIPY Dye Fluorescence Lifetimes

Fluorescence lifetime decays were measured at the University of Zurich using a custom-built instrument described previously.[7] Picosecond light pulses from a white light source (SC-450-4, 20 MHz, Fianium, Southampton, UK) were used for excitation. The excitation wavelengths were selected by HQ470/40 (Chroma) and z582/15 (Semrock) bandpass filters. The binning width of the recorded histograms is 4 ps.

Cavitands **3** and **1a** were employed to measure the mean fluorescence lifetimes τ_D and τ_A. The donor dye decay curve of cavitand **3** after donor excitation with $\lambda_{exc} = 470$ nm, and the acceptor dye decay curve of cavitand **1a** after acceptor excitation with $\lambda_{exc} = 582$ nm are presented below. The curves were fitted with monoexponential decay functions convolved with the instrument response functions (IRF), yielding the mean fluorescence lifetimes $\tau_D = 4.21$ ns and $\tau_A = 5.24$ ns.

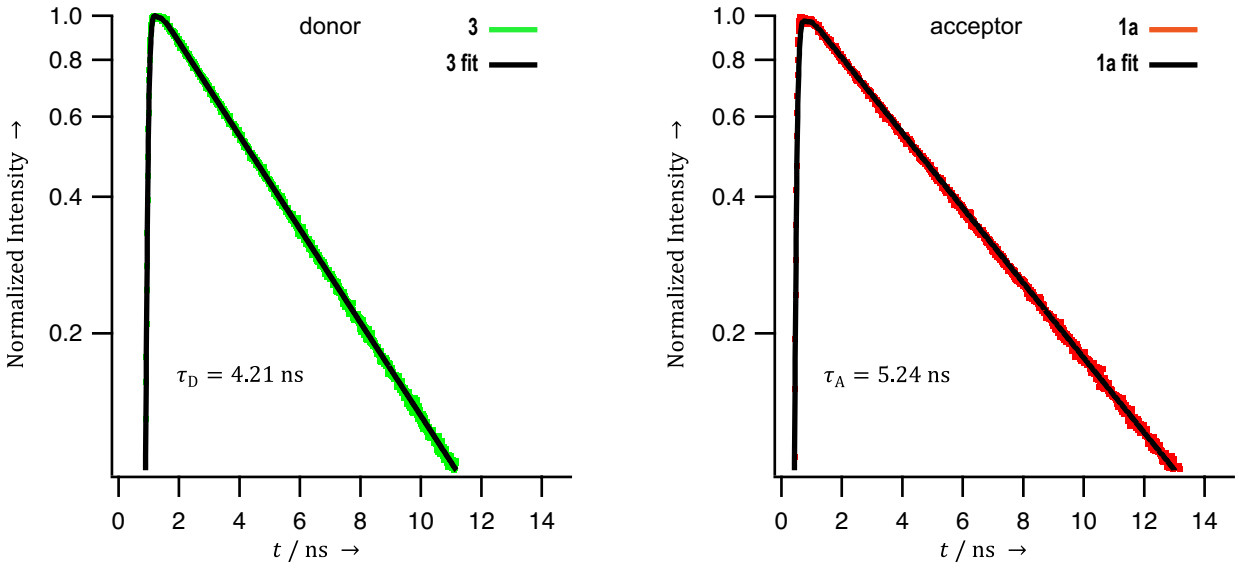

Figure S5. Fluorescence decay curves of reference donor cavitand **3** (left) excited with $\lambda_{exc} = 470$ nm, and selectively excited acceptor of cavitand **1a** (right) with $\lambda_{exc} = 582$ nm. Measurements were performed under magic angle configuration i.e. emission polarizer set to 54.7° with respect to excitation polarization. Monoexponential decay fitting yielded mean fluorescence lifetimes $\tau_D = 4.21$ ns for the donor BODIPY dye and $\tau_A = 5.24$ ns for the acceptor BODIPY dye.

3.2 Discussion on Potential Electron Transfer

While electron-poor quinones can act as electron acceptors, in case of our quinone moieties the acceptor property is diminished due to electron-donation from the O-atoms of the cavitand backbone; the first redox potential of the quinone moiety was recorded at −1.1 V.[8] In addition, owing to the stiffness of the linker, direct contact between the quinone walls and the dyes through space is essentially impossible, and electron transfer through the linker arm is very unlikely. Electron transfer from the quinone moieties to the excited dyes would also be accompanied by broad, red-shifted charge-transfer bands in the fluorescence spectra of the cavitands. The absence of such bands is another argument against the occurrence of electron transfer in these molecules. Finally, Figure S6 below shows quantum yields (QY) of relevant single BODIPY dyes **6**–**8** and cavitands **1a**–**d** (Details on the determination of the quantum yields are reported in Section 3.4 of the Supporting Information). The QYs are independent of the length of the linker, which also strongly argues against electron transfer to the quinone walls. In summary, electron transfer from the chromophoric group to the quinone groups does not have to be taken into account for our analysis.

Concerning potential photoinduced electron transfer between the two BODIPY dyes, this energetics can be estimated with the Rehm-Weller-equation, which takes into account the redox potentials of the donor and acceptor dyes. The redox potentials of the BODIPY dyes used in this study were previously measured (see Figure S6 below). Further required parameters are the excited state energy of the $S_0 \rightarrow S_1$ transition of the donor (E_{00} = 2.33 eV, calculated from the wavelength of the absorption maximum of the donor dye, λ_{max} = 529 nm) and a work term of 0.3 eV (empirical coulombic factor for non-polar solvents). Using these data, we obtain a Gibbs free energy of ΔG = 1.2 kcal mol^{-1} for the photoinduced electron transfer from the excited donor to the acceptor dye. On the other hand, we obtain ΔG = 3.9 kcal mol^{-1} for the photoinduced electron transfer from the acceptor to the excited donor. Both processes are thus endergonic. Not only is electron transfer between the donor and acceptor BODIPY dyes in the closed cavitands unlikely due to thermodynamic reasons, electron transfer has even more stringent requirements for the distance between the two dyes (i.e. if electron transfer does take place, Förster transfer will be extremely efficient also). Possible electron transfer would therefore not have any bearing on the central conclusion regarding the vase cavitands, which is that the opening angle is close to

zero. In the kite cavitand, the distance between donor and acceptor is clearly too large for electron transfer to occur.

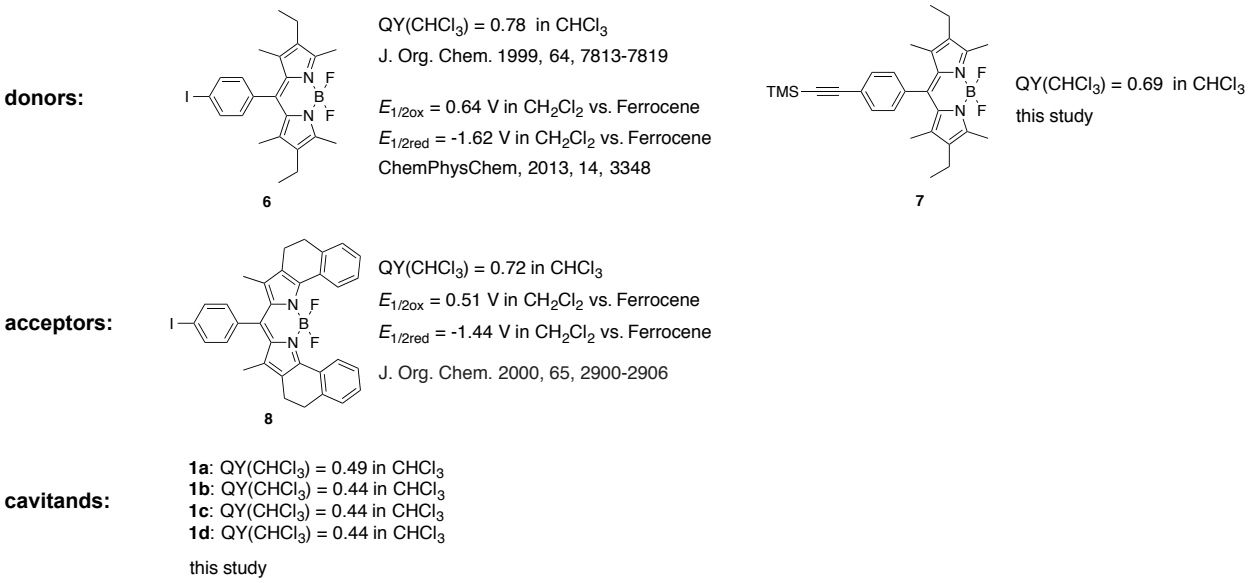

Figure S6. Quantum yields and redox potentials of relevant BODIPY dyes **6**–**8** and cavitands **1a**–**d**.

3.3 Determination of Quantum Yields and Förster Radius R_0

Measurements of quantum yields (QY) and determination of R_0 were carried out in the Beckman Institute Laser Resource Center (California Institute of Technology) and were supported by the Arnold and Mabel Beckman Foundation. All QY's were measured at concentrations of <1 μM in chloroform at room temperature and in ambient air. Solid samples were stored in the dark and refrigerated, solutions were prepared directly before taking data. Maximum peak absorptions did not exceed 0.25 to avoid detrimental self-absorption effects. UV/Vis absorption spectra were collected with a Cary 50 UV/Vis spectrophotometer in 1 cm pathlength quartz cuvettes. The acceptor extinction coefficient was determined in the following way: Four small amounts of acceptor (**9**, Figure S8) were weighed out and dissolved in known volumes of chloroform. The optical spectra of these solutions of known concentrations were measured and the average extinction coefficient of **9** was calculated using Beer's law. Emission spectra were recorded on a Jobin Yvon Spec Fluorolog-3-11. Samples were excited with 532-nm light, which was provided by a xenon arc lamp equipped with a monochromator for wavelength selection. Right angle emission was diffracted with a monochromator and detected with a Hamamatsu R928P photomultiplier tube with photon counting.

QY data of samples **1a**–**d** and **7** were collected using the comparative method of Williams *et al.*[9] This method involves the use of a well-characterized standard sample (here: anthracene in ethanol) with a known QY value. The measured QY data are summarized in Figure S7.

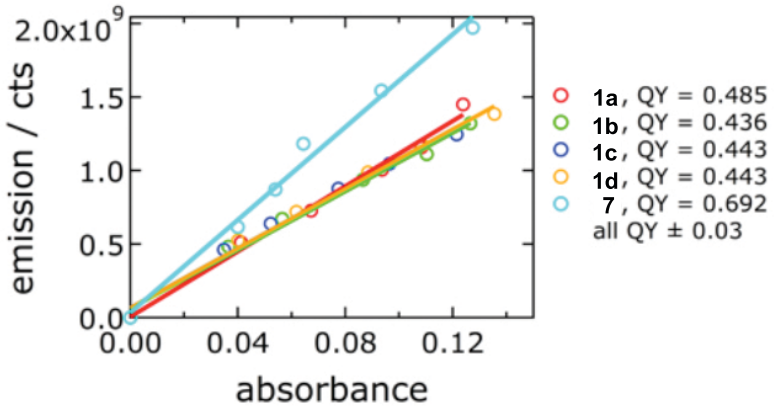

Figure S7. Measured integrated fluorescence intensity vs. absorbance (circles). The solid lines are linear fits with the slope *m* and the intercept 0.

QY's were derived by comparison to a known value in the following way: The slopes *m* of the unknown substances (*x*) and standard (*std*) were measured as described above. The QY of an unknown substance (*x*) is given by the equation below, in which *n* denotes the index of refraction of the solvent.

$$QY_x = QY_{std} \cdot \left(\frac{m_x}{m_{std}}\right) \cdot \left(\frac{n_x^2}{n_{std}^2}\right)$$

The Förster radius R_0 was determined using the equations below and the measured acceptor extinction spectrum (experimental details see above).

Donor: $$R_0^6 = \frac{9\,\mathrm{QY}_D(\ln 10)\kappa^2 J}{128\,\pi^5 n^4 N_A}$$

$\kappa^2 = 2/3$ random orientation of donor molecules in solution

$n = 1.4460$ refractive index of chloroform

N_A : Avogadro's number

$$J = \int f_D(\lambda)\epsilon_A(\lambda)\lambda^4\,\mathrm{d}\lambda$$

f_D : normalized donor fluorescence spectrum

ϵ_A : acceptor molar extinction spectrum

λ : wavelength

The acceptor (**9**) extinction and normalized donor (**7**) emission spectra are depicted in Figure S8.

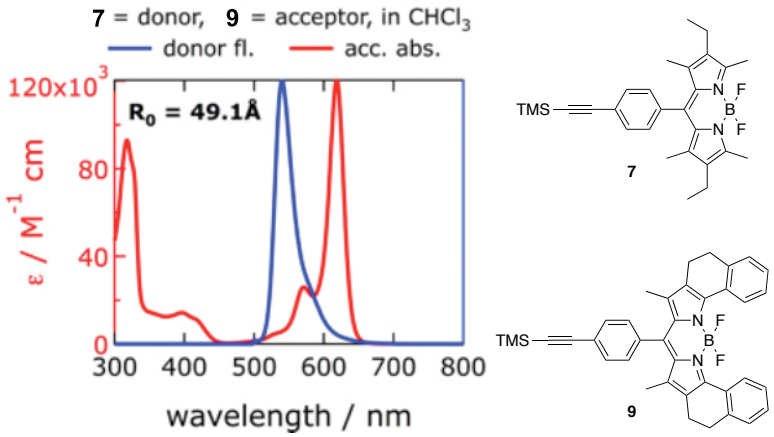

Figure S8. Acceptor extinction (**9**, red) and normalized donor emission (**7**, blue) spectra.

A Förster radius R_0 = 49.1 Å was obtained from steady-state absorption and emission spectra, and the equation above was used; κ^2 was assumed to be 2/3, which is a good approximation for a random orientation of donor and acceptor molecules in solution.

3.4 Analysis of Decay Curves

The fluorescence decay curves of the donor dyes in cavitands **1a**–**d** show multiexponential behavior whose description requires at least two decay times. The results of biexponential fits are shown in the Table below.

Table S1. Biexponential fits of the fluorescence decay curves of the donor moieties of cavitands **1a**–**d**

cavitand	τ_1 / ns	τ_2 / ns
1a	0.3	3.8
1b	0.5	3.9
1c	0.5	3.7
1d	0.8	3.8

Fitted with IRF-convolution

4 MD Setup

4.1 Preparation of GAFF Input Files

Cavitands and linker molecules were assembled from HF/6-31G(d)-optimized fragments. Atom charges were calculated with the restrained electrostatic potential (RESP) fitting method of the molecular electrostatic potential (MEP),[10] performed on the RED Server[11] (development version 2012; allows to input up to 350 atoms) with the charge model RESP-A1A (HF/6-31G(d)//HF/6-31G(d) – Connolly surface algorithm used in MEP computation – 2 stage RESP fit qwt = 0.0005/0.001), using the Gaussian 09 software[12]. Bonded and non-bonded parameters were assigned with the program ACPYPE,[13] which interfaces with the program ANTECHAMBER.[14] Bonded and non-bonded parameters involving the boron atoms were taken from parameters derived for CHARMM,[15] and ported to GROMACS by means of unit conversion. Chloroform parameters (GAFF) and liquid structure coordinates were obtained from virtualchemistry.org.[16]

4.2 Preparation of CGenFF Input Files

Cavitands and linker molecules were parameterized for CGenFF (version 2b7) via ParamChem Web service (www.paramchem.org, version 0.9.6).[17] Bonded and non-bonded parameters involving the boron atoms were taken from literature.[15] Chloroform parameters (OPLS) and liquid structure coordinates were obtained from virtualchemistry.org.[16]

4.3 MD Run Parameters.

Cavitands or linker molecules, respectively, were solvated in a box of pre-equilibrated chloroform molecules with a minimal distance of 13 Å between any atom of the solute and the periodic boundary. As the guest-exchange rate for 2,6-dimethylphenyl-substituted cavitands is slow on the NMR timescale,[18] we expected that chloroform molecules would not diffuse into the cavity on the MD simulation timescale by itself. Therefore, one chloroform molecule was manually placed into the cavities of cavitands **1a**–**d**. It was observed that this chloroform molecule remained in the cavity throughout the whole simulation. The simulation time was 500 ns for cavitands and 100 ns for linker molecules, with a time step of 1 fs (such a short time step is required due to the high vibrational frequency of triple bonds present in linker units). Cavitand coordinates were saved every 4 ps and linker molecule coordinates every 5 ps. Long-

range electrostatics and van der Waals interactions were treated with a simple cut-off scheme using PME and a cut-off at 10 Å.[19] The temperature was kept constant at 298 K by applying the Velocity Rescaling algorithm.[19] The system pressure was kept constant at 1 atm with the Parinello Rahman Barostat.[19] The LINCS algorithm was used to keep all bonds involving hydrogen atoms constrained.[19] All molecular dynamics simulations were performed with a Message Passing Interface (MPI) version of GROMACS v. 4.5.5.[20] Simulations were performed on the Brutus super computer,[21] employing 16 cores per simulation. The total simulation time accumulated over all simulations was 5 μs for the cavitand and 0.8 μs for the linker molecules. Atom coordinates were extracted from each snapshot via the g_traj routine of GROMACS, and subsequent calculations were performed with the Python programming language version 2.7.

5 Fluorescence Decay Curves from MD Data

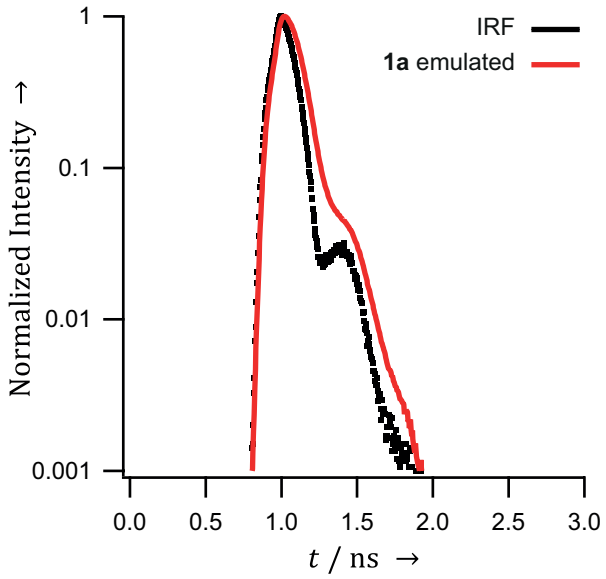

Figure S9. Donor fluorescence emission decay curve of vase cavitand **1a** with an implemented donor-only fraction of 0% emulated on the basis of a CGenFF-simulation trajectory: an extremely rapid decay is observed that basically parallels the IRF, if a donor-only fraction is not taken into account for the emulation.

6 Linker Study

We subjected molecules **13a**–**d**[22] (Figure S10, O˙ was replaced by H) to MD simulations with CGenFF and GAFF (explicit chloroform, 100 ns each).

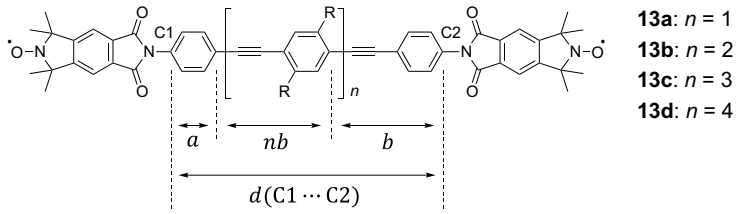

Figure S10. Test compounds **13a**–**d** used in literature to determine the persistence length of a phenylene-ethynylene-based polymer to be $L_p = 13.8 \pm 1.5$ nm.[22] We used these test compounds to determine and compare the persistence lengths resulting from MD simulations with CGenFF and GAFF.

The obtained $d(\mathrm{C1} \cdots \mathrm{C2})$ distance distribution histograms are illustrated in Figure S11. The histograms obtained with CGenFF are broader than the ones obtained with GAFF, indicating that GAFF parameters result in stiffer phenylene-ethynylene linkers than CGenFF parameters. Quantification of L_p values from MD data can be achieved by applying the Worm-Like Chain (WLC) model, which is often used to describe the behavior of semi-flexible polymers.[23] According to the WLC model, the mean square end-to-end distance $\langle R^2 \rangle = \langle d(\mathrm{C1} \cdots \mathrm{C2}) \rangle$ of a chain can be described by Equation:[22a]

$$\langle R^2 \rangle = 2 c_l L_p \left(1 - \frac{L_p}{c_l} \left(1 - e^{-\frac{c_l}{L_p}} \right) \right) \qquad (1)$$

where c_l is the contour length – the $\langle d(\mathrm{C1} \cdots \mathrm{C2}) \rangle$ distance of the chain in its stretched, linear form. The contour lengths of systems **13a**–**d** are composed of one phenyl unit with the length a, and $(n+1)$ phenylene-ethynylene units with the length b (Figure S10). Thus, the compound-specific c_l values of **13a**–**d** can be described according to:

$$c_l(n) = a + (n+1)b \qquad (2)$$

The parameters a and b are force field-specific and were therefore used as fit parameters together with L_p. Substituting Equation (2) in (1) yields:

$$\langle R^2\rangle(n) = 2(a+(n+1)b)L_p\left(1-\frac{L_p}{a+(n+1)b}\left(1-e^{-\frac{a+(n+1)b}{L_p}}\right)\right) \qquad (3)$$

Equation (3) was used to fit the $\langle R^2\rangle(n)$ values obtained by CGenFF and GAFF, with a, b, and L_p as fit parameters. The resulting plots and fits are illustrated in Figure S12.

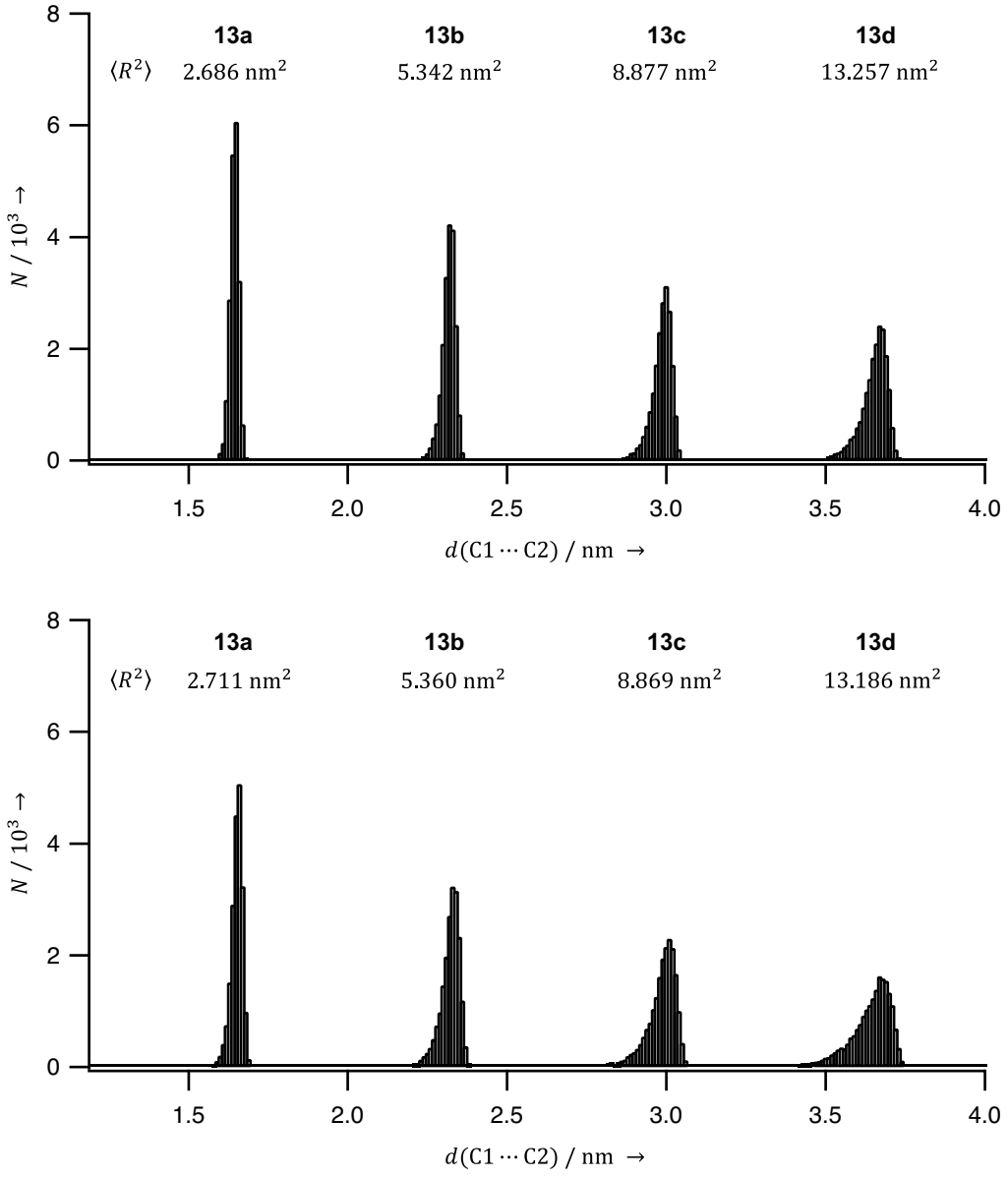

Figure S11. Histograms of distances $\langle d(\mathrm{C1}\cdots\mathrm{C2})\rangle$ in test compounds **13a–d** obtained from MD simulations with GAFF (top) and CGenFF (bottom). $\langle R^2\rangle = \langle d(\mathrm{C1}\cdots\mathrm{C2})\rangle$.

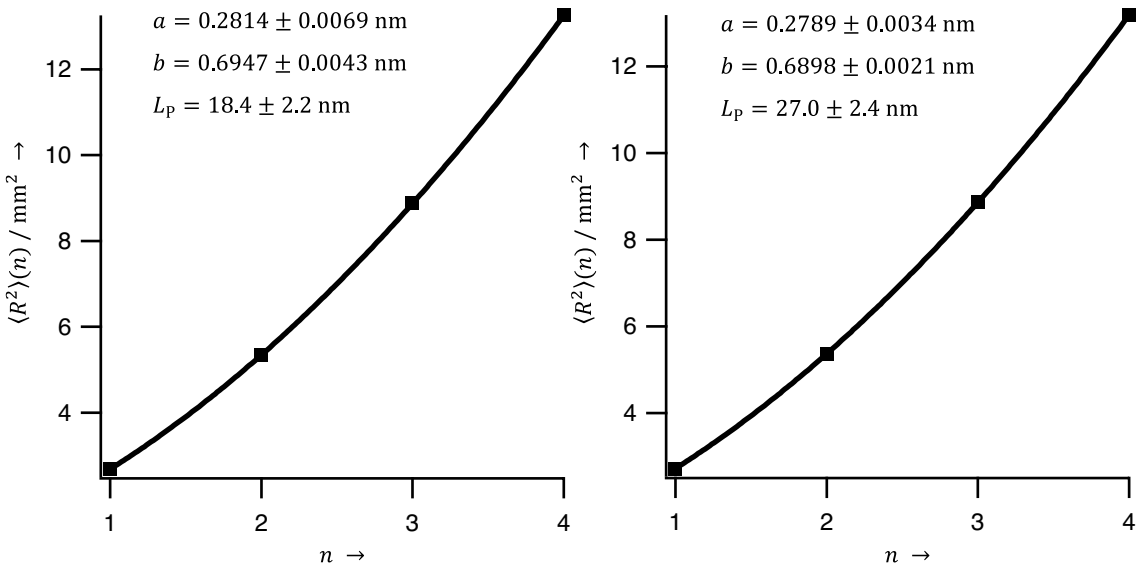

Figure S12. Plots of the mean square end-to-end distances $\langle R^2 \rangle$ against the number of phenylene-ethynylene linker units n in test compounds **13a**–**d** simulated with CGenFF (left) and GAFF (right). The plots were fitted to Equation (3) to determine the contour lengths L_p.

7 NMR Spectra of the Products

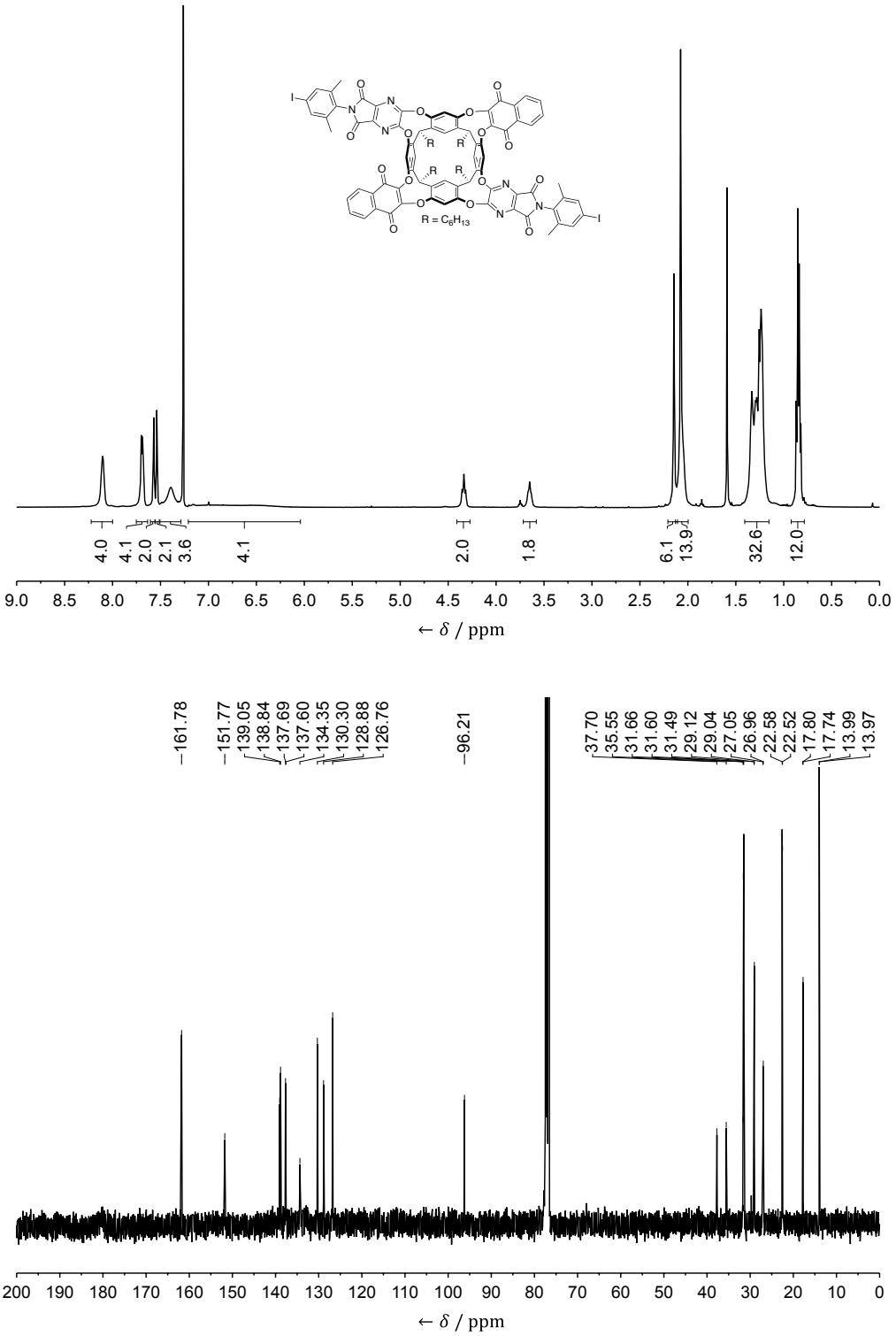

Figure S13. ^{1}H NMR (top, 400 MHz) and ^{13}C NMR (bottom, 100 MHz) spectra of compound **5** in $CDCl_3$ at 298 K.

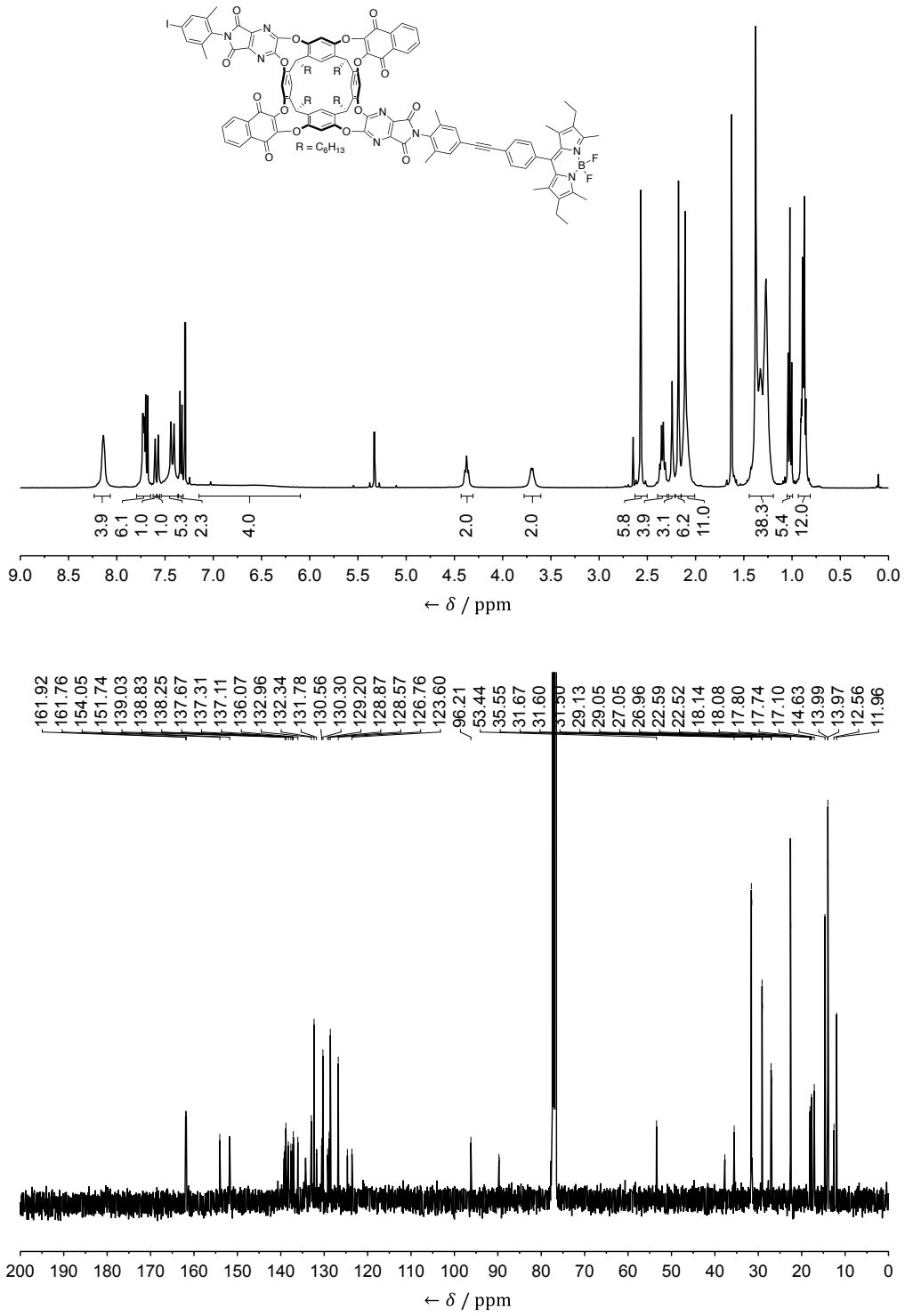

Figure S14. ^{1}H NMR (top, 400 MHz) and ^{13}C NMR (bottom, 100 MHz) spectra of compound **11** in $CDCl_3$ at 298 K.

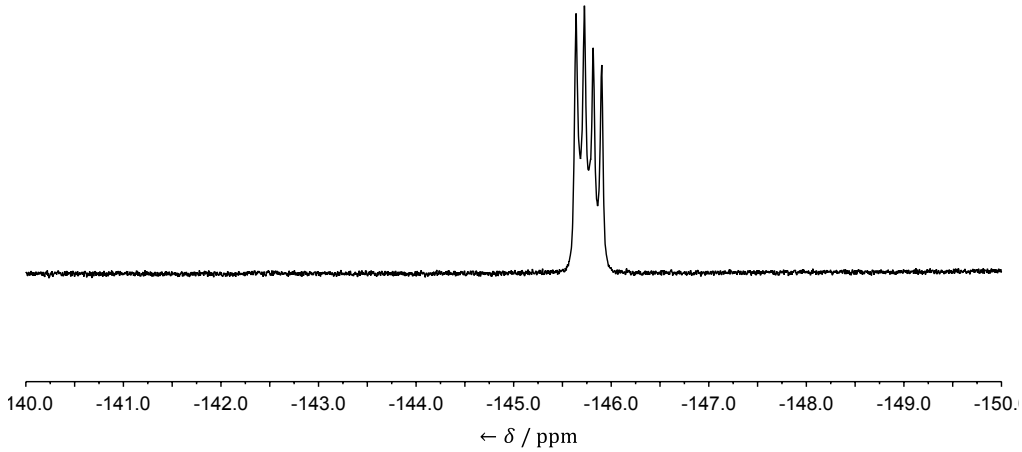

Figure S15. ^{19}F NMR (376 MHz) spectrum of compound **11** in $CDCl_3$ at 298 K.

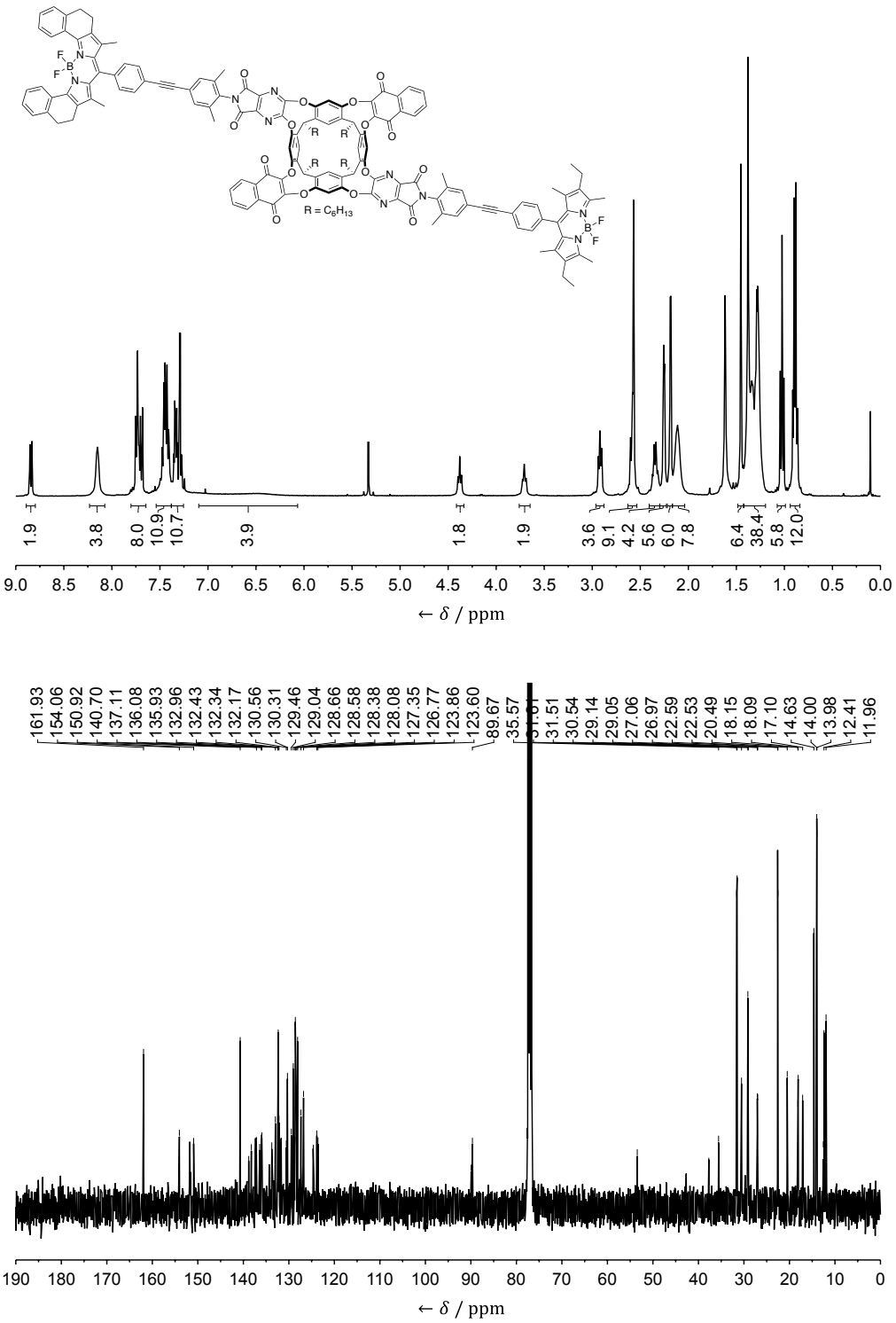

Figure S16. ^{1}H NMR (top, 400 MHz) and ^{13}C NMR (bottom, 100 MHz) spectra of compound **2** in $CDCl_3$ at 298 K.

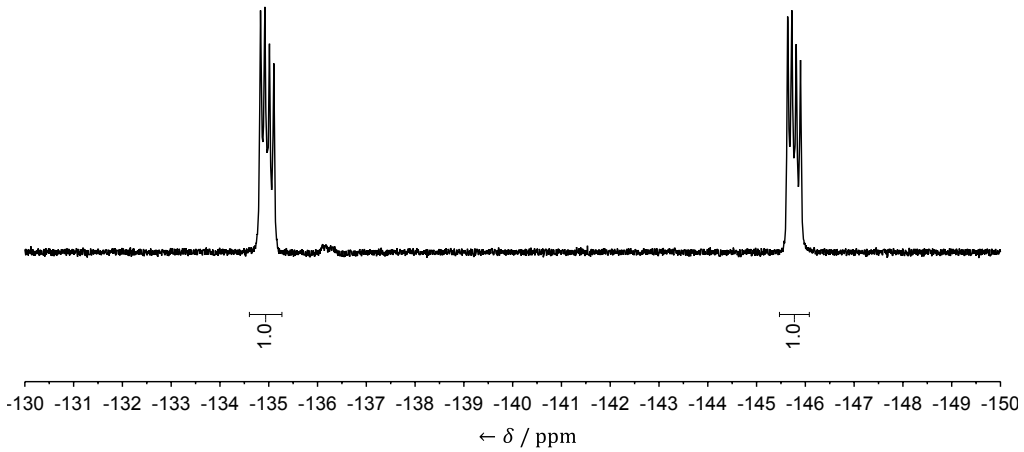

Figure S17. ^{19}F NMR (376 MHz) spectrum of compound **2** in $CDCl_3$ at 298 K.

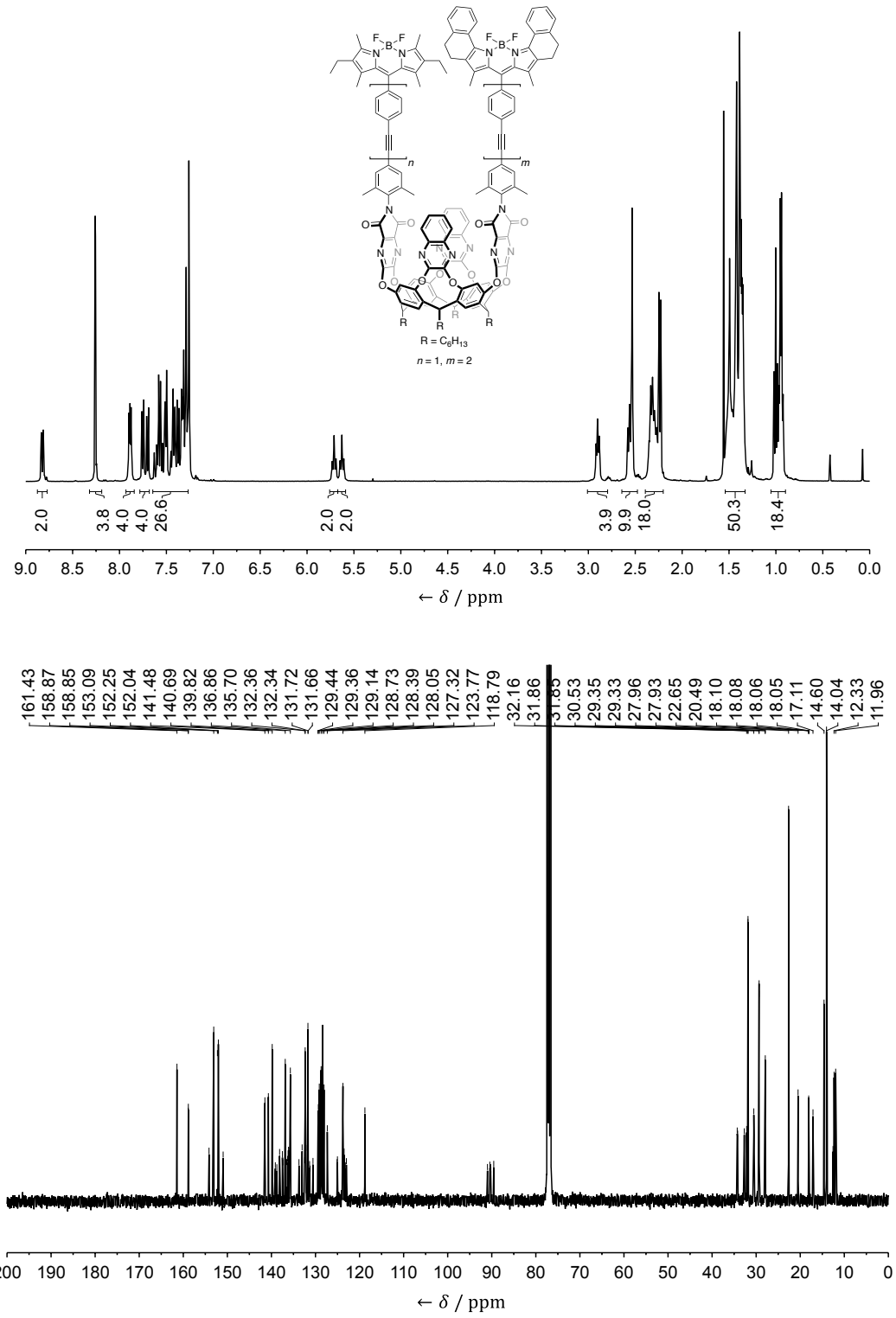

Figure S18. ^{1}H NMR (top, 400 MHz) and ^{13}C NMR (bottom, 100 MHz) spectra of compound **1d** in $CDCl_3$ at 298 K.

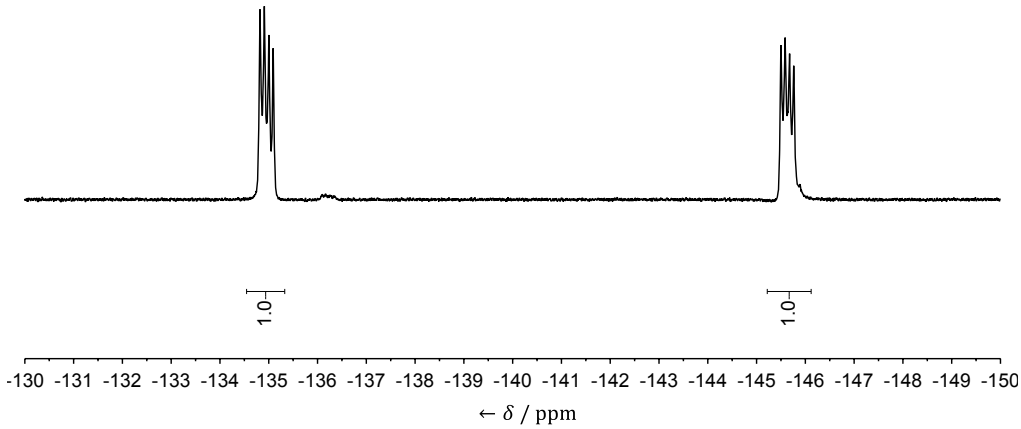

Figure S19. ^{19}F NMR (376 MHz) spectrum of compound **1d** in $CDCl_3$ at 298 K.

8 References

(1) Pochorovski, I.; Breiten, B.; Schweizer, W. B.; Diederich, F., *Chem. Eur. J.* **2010**, *16*, 12590.

(2) Azov, V. A.; Schlegel, A.; Diederich, F., *Bull. Chem. Soc. Jpn.* **2006**, *79*, 1926.

(3) Pochorovski, I.; Ebert, M.-O.; Gisselbrecht, J.-P.; Boudon, C.; Schweizer, W. B.; Diederich, F., *J. Am. Chem. Soc.* **2012**, *134*, 14702.

(4) Azov, V. A.; Schlegel, A.; Diederich, F., *Angew. Chem. Int. Ed.* **2005**, *44*, 4635.

(5) (a) Liras, M.; Prieto, J. B.; Pintado-Sierra, M.; Arbeloa, F. L.; García-Moreno, I.; Costela, Á.; Infantes, L.; Sastre, R.; Amat-Guerri, F., *Org. Lett.* **2007**, *9*, 4183; (b) Bañuelos, J.; López Arbeloa, F.; Arbeloa, T.; Salleres, S.; Vilas, J. L.; Amat-Guerri, F.; Liras, M.; López Arbeloa, I., *J. Fluoresc.* **2008**, *18*, 899.

(6) (a) Crawford, S. M.; Thompson, A., *Org. Lett.* **2010**, *12*, 1424; (b) Smithen, D. A.; Baker, A. E. G.; Offman, M.; Crawford, S. M.; Cameron, T. S.; Thompson, A., *J. Org. Chem.* **2012**, *77*, 3439.

(7) Nettels, D.; Hoffmann, A.; Schuler, B., *J. Phys. Chem. B* **2008**, *112*, 6137.

(8) Pochorovski, I.; Boudon, C.; Gisselbrecht, J.-P.; Ebert, M.-O.; Schweizer, W. B.; Diederich, F., *Angew. Chem. Int. Ed.* **2012**, *51*, 262.

(9) Williams, A. T. R.; Winfield, S. A.; Miller, J. N., *The Analyst* **1983**, *108*, 1067.

(10) Bayly, C. I.; Cieplak, P.; Cornell, W.; Kollman, P. A., *J. Phys. Chem.* **1993**, *97*, 10269.

(11) (a) Dupradeau, F.-Y.; Pigache, A.; Zaffran, T.; Savineau, C.; Lelong, R.; Grivel, N.; Lelong, D.; Rosanski, W.; Cieplak, P., *Phys. Chem. Chem. Phys.* **2010**, *12*, 7821; (b) Vanquelef, E.; Simon, S.; Marquant, G.; Garcia, E.; Klimerak, G.; Delepine, J. C.; Cieplak, P.; Dupradeau, F.-Y., *Nucl. Acids Res.* **2011**, *39*, W511.

(12) Frisch, M. J.; Trucks, G. W.; Schlegel, H. B.; Scuseria, G. E.; Robb, M. A.; Cheeseman, J. R.; Scalmani, G.; Barone, V.; Mennucci, B.; Petersson, G. A.; Nakatsuji, H.; Caricato, M.; Li, X.; Hratchian, H. P.; Izmaylov, A. F.; Bloino, J.; Zheng, G.; Sonnenberg, J. L.; Hada, M.; Ehara, M.; Toyota, K.; Fukuda, R.; Hasegawa, J.; Ishida, M.; Nakajima, T.; Honda, Y.; Kitao, O.; Nakai, H.; Vreven, T.; Montgomery, J., J. A.; Peralta, J. E.; Ogliaro, F.; Bearpark, M.; Heyd, J. J.; Brothers, E.; Kudin, K. N.; Staroverov, V. N.; Kobayashi, R.; Normand, J.; Raghavachari, K.; Rendell, A.; Burant, J. C.; Iyengar, S. S.; Tomasi, J.; Cossi, M.; Rega, N.; Millam, J. M.; Klene, M.; Knox, J. E.; Cross, J. B.; Bakken, V.; Adamo, C.; Jaramillo, J.; Gomperts, R.; Stratmann, R. E.; Yazyev, O.; Austin, A. J.; Cammi, R.; Pomelli, C.; Ochterski, J. W.; Martin, R. L.;

Morokuma, K.; Zakrzewski, V. G.; Voth, G. A.; Salvador, P.; Dannenberg, J. J.; Dapprich, S.; Daniels, A. D.; Farkas, Ö.; Foresman, J. B.; Ortiz, J. V.; Cioslowski, J.; Fox, D. J., Gaussian 09 Revision A.1, Gaussian, Inc., Wallingford CT, 2009.

(13) Sousa da Silva, A.; Vranken, W., *BMC Res. Notes* **2012**, *5*, 367.

(14) (a) Wang, J.; Wolf, R. M.; Caldwell, J. W.; Kollman, P. A.; Case, D. A., *J. Comput. Chem.* **2004**, *25*, 1157; (b) Wang, J.; Wang, W.; Kollman, P. A.; Case, D. A., *J. Mol. Graph. Model.* **2006**, *25*, 247.

(15) Song, K. C.; Livanec, P. W.; Klauda, J. B.; Kuczera, K.; Dunn, R. C.; Im, W., *J. Phys. Chem. B* **2011**, *115*, 6157.

(16) Caleman, C.; van Maaren, P. J.; Hong, M.; Hub, J. S.; Costa, L. T.; van der Spoel, D., *J. Chem. Theory Comput.* **2012**, *8*, 61.

(17) (a) Vanommeslaeghe, K.; Mackerell, J., A D, *J. Chem. Inf. Model.* **2012**, *52*, 3144; (b) Vanommeslaeghe, K.; Raman, E. P.; Mackerell, J., A D, *J. Chem. Inf. Model.* **2012**, *52*, 3155.

(18) Shirtcliff, L. D.; Xu, H.; Diederich, F., *Eur. J. Org. Chem.* **2010**, 846.

(19) van der Spoel, D.; Lindahl, E.; Hess, B.; van Buuren, A. R.; E. Apol, P. J. M.; Tieleman, D. P.; Sijbers, A. L. T. M.; Feenstra, K. A.; van Drunen, R.; Berendsen, H. J. C., Gromacs User Manual version 4.5.5.

(20) (a) Hess, B.; Kutzner, C.; van der Spoel, D.; Lindahl, E., *J. Chem. Theory Comput.* **2008**, *4*, 435; (b) van der Spoel, D.; Lindahl, E.; Hess, B.; Groenhof, G.; Mark, A. E.; Berendsen, H. J. C., *J. Comput. Chem.* **2005**, *26*, 1701; (c) Lindahl, E.; Hess, B.; van der Spoel, D., *J. Mol. Model.* **2001**, *7*, 306; (d) Berendsen, H. J. C.; van der Spoel, D.; van Drunen, R., *Comput. Phys. Commun.* **1995**, *91*, 43.

(21) Brutus Cluster. https://www1.ethz.ch/id/services/list/comp_zentral/cluster/index_EN.

(22) (a) Jeschke, G.; Sajid, M.; Schulte, M.; Ramezanian, N.; Volkov, A.; Zimmermann, H.; Godt, A., *J. Am. Chem. Soc.* **2010**, *132*, 10107; (b) Godt, A.; Schulte, M.; Zimmermann, H.; Jeschke, G., *Angew. Chem. Int. Ed.* **2006**, *45*, 7560.

(23) Kratky, O.; Porod, G., *Recl. Trav. Chim. Pay-B* **1949**, *68*, 1106.